Biobased Antimicrobial Coatings: Layer-by-Layer Assemblies Based on Natural Polyphenols

ACS APPLIED POLYMER MATERIALS

pubs.acs.org/acsapm
Article

Biobased Antimicrobial Coatings: Layer-by-Layer Assemblies Based on Natural Polyphenols

Pavel Vostrejs, Adriana Kovalcik,* Jana Bianca Schaubeder, Stefan Spirk, Michal Hricovini, Tiina Nypelö, Michal Kalina, Nicole Cernekova, Matej Brezina, and Rupert Kargl

Cite This: ACS Appl. Polym. Mater. 2025, 7, 3601−3610
Read Online

ACCESS | Metrics & More | Article Recommendations | Supporting Information

ABSTRACT: Natural polyphenols possess inherent defensive properties against pathogens. This study investigated the radical scavenging and antimicrobial activity of biobased polyphenol nanoparticles (PNPs) derived from grape seeds. Scanning electron micrographs and dynamic light scattering confirmed the synthesized nanoparticles' spherical shape, showing an average hydrodynamic radius of 93.9 ± 4.0 nm. The PNPs exhibited radical scavenging activity at about 433 mg Trolox per gram and a microbial inhibitory effect against *Micrococcus luteus* and *Escherichia coli*. The negatively charged PNPs were used to prepare thin multilayer films combined with positively charged polyelectrolytes such as poly(allylamine hydrochloride), poly-L-lysine, poly(diallyldimethylammonium chloride), or polyethylenimine. The viscoelastic properties of polyelectrolyte/PNP films were monitored using a quartz crystal microbalance with dissipation. The PNPs showed the best interface compatibility with poly-L-lysine (PLL), enabling the preparation of mechanically stable thin multilayer films. The antioxidant activity of PLL/PNP films was 72 ± 6 μg Trolox per cm^2 at pH 10. The PLL/PNP films displayed antimicrobial activity against *M. luteus* and *E. coli*, with growth inhibition of 50.7 ± 0.6% and 12.1 ± 0.6%, respectively. The prepared biobased PLL/PNP Layer-by-Layer assemblies can potentially prevent biofilm formation on a large spectrum of materials.

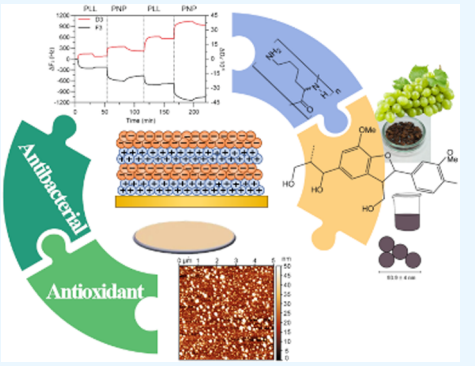

KEYWORDS: *antioxidant activity, antibacterial activity, films, interface, polyphenols, polyelectrolytes*

1. INTRODUCTION

The formation of bacterial biofilms on surfaces in medical equipment or hospitals generally complicates patient treatment. Despite consistent and rigorous surface sanitation, the problem is partly attributed to the growing resistance of pathogenic microorganisms to traditional safety and good manufacturing practices.[1] Recent research has shown that the development of active antimicrobial surface coatings can effectively prevent microbial biofilm formation on various surfaces.[2]

Antimicrobial substances can be isolated from many microorganisms, plants, and animals.[3] In the context of society's current efforts to support the circular economy approach, lignocellulosic biomass is a valuable material for discovering and isolating substances with antioxidant and/or antimicrobial activity.[4,5] Lignocellulosic biomass such as wood, agricultural, and plant residues contain cellulose, hemicellulose, lignin, and other phenolic compounds. Phenolic compounds, including lignin, flavonoids, and tannins, are plant secondary metabolites with antioxidant and/or antimicrobial activity.[6]

Agricultural byproducts such as grape pomace are among the valuable materials containing polyphenols. Agricultural byproducts such as grape pomace from the wine industry are among the sought-after and important materials containing polyphenols. In the case of grape pomace recovery, it is advantageous to divide them into two groups: (1) seeds and (2) skins, stems, and pulp. Grape seeds and skin are precious sources of polyphenols. Duba et al. reported polyphenol yields of 124 ± 1 mg g^{-1} for grape seeds and 77 ± 3 mg g^{-1} for grape skins.[7] In addition to phenolic compounds (catechin, epicatechin, procyanidins, phenolic acids, and lignin), grape seeds contain oils, cellulose and hemicellulose, extractives and ash.[8,9] Although the health benefits of the functional components of grape seeds have been confirmed, they are usually incinerated or end up in landfills after the grapes have been pressed because they have no further value to the winemakers.[10−13] In our previous work, we introduced the concept of a biorefinery to isolate and produce value-added products from grape pomace. We have shown that grape winery residues are a promising feedstock for producing

Received: November 22, 2024
Revised: March 2, 2025
Accepted: March 5, 2025
Published: March 14, 2025

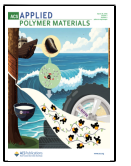

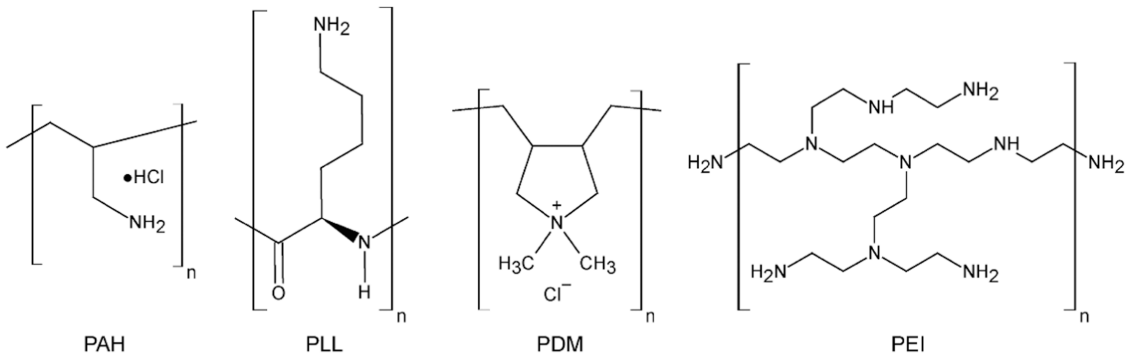

Figure 1. List of polyelectrolytes used for the preparation of LbL assemblies with PNP (polyphenol nanoparticles): poly(allylamine hydrochloride) (PAH), poly-L-lysine (PLL), Poly(diallyldimethylammonium chloride) (PDM) and polyethylenimine (PEI).

biodegradable polyesters such as polyhydroxyalkanoates and other value-added products, including grape oil and lignin.[14]

A large part of polyphenols present in grape pomace is lignin, for which the extraction method is established in laboratory praxis.[9,15,16] Unfortunately, these lignin extracts are heterogeneous and composed of phenolic compounds, carbohydrates, and other constituents that limit their utilization.[17] The chemical structure of lignin is related to several factors, such as the natural source of lignin-containing lignocellulosic materials, growth conditions, the isolation method, and postprocess modification.[18] The strong interactions between lignin and proanthocyanidins have been confirmed in the grape seeds.[19] It is supposed that lignin isolated from grape seeds is a lignin complex with proanthocyanidins.

Synthesis of lignin nanoparticles is a possibility for preparing materials with pharmaceutical purity, thus enlarging their applicability.[20] Lignin in the form of nanoparticles may be processed into ultra-thin films, for example, by spin coating on a specific substrate or by direct adsorption of lignin nanoparticles onto a particular substrate.[21−23] A good adhesive strength of lignin on different surfaces (stainless steel, aluminum, wood, polypropylene) can be reached by the formation of complexes with cationic polyelectrolytes such as poly(allylamine hydrochloride) (PAH) and ε-poly-L-lysine (PLL).[24−26] The fabricating of multilayer thin films with controlled architecture and interface was proven using a layer-by-layer (LbL) assembly methodology.[25−27]

To further explore this field, our study presents an approach for creating antioxidant and antimicrobial multilayer coatings using grape seed polyphenol nanoparticles and cationic polyelectrolytes. We hypothesize that selecting the appropriate positively charged polyelectrolytes would enhance the interaction and compatibility with polyphenolic nanoparticles (PNPs) derived from grape seed lignin. To test this, we determined phenolic nanoparticles' interaction and compatibility with cationic polyelectrolytes using quartz-crystal microbalance with dissipation (QCM-D) measurements and atomic force microscopy (AFM).

We hypothesize that polyphenol nanoparticles with high compatibility with polyelectrolytes would form multilayer thin films with favorable viscoelastic properties, high antioxidant capacity and antimicrobial activity. To validate this hypothesis, polyphenolics were extracted from grape seeds and precipitated into nanoparticles. The polyphenol nanoparticles/polyelectrolyte thin films were prepared using the LbL method on a gold surface, and their viscoelastic properties, radical scavenging capacity and antimicrobial activity were investigated.

2. EXPERIMENTAL SECTION

2.1. Materials. Poly(allylamine hydrochloride) (PAH) average M_w 50,000 g mol^{-1}, lot #283223, poly-L-lysine (PLL) 1 g L^{-1} solution lot #P8920, poly(diallyldimethylammonium chloride) (PDM) solution average M_w 200,000−350,000 g mol^{-1}, lot #409022, polyethylenimine (PEI) ethoxylated solution lot #423475, 2,2′-azino-bis(3-ethylbenzothiazoline-6-sulfonic acid) (ABTS), potassium persulfate, and gallic acid monohydrate ≥98% were all supplied by Sigma-Aldrich (Germany). KBr and LiBr were purchased from VWR, Germany. Dimethyl sulfoxide 99.9%, Tetrahydrofuran 99.5%, and *n*-hexane 99% were supplied by Carl Roth GmbH (Germany).

Colloidal polyphenol nanoparticles (PNPs) were synthesized from grape seed lignin (GSL) using the methodology described by Sipponen et al.[28] Details concerning grape seed lignin isolation and composition are shown in the Supporting Information (Table S1).

The thin multilayer films were prepared by layering PNPs and polyelectrolytes (PEs) (Figure 1) on gold sensors (QSX-301), while the LbL assembly method was introduced (Figure 2). PEs were titrated to determine the charging isotherms as published elsewhere (Figure S5).[29]

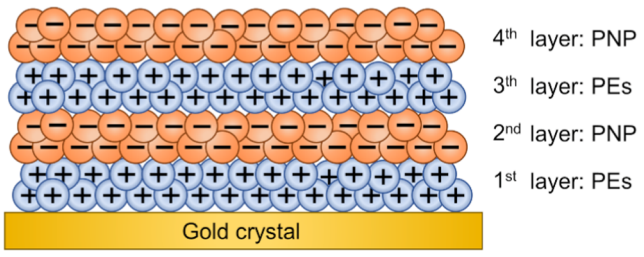

Figure 2. Scheme of the layer-by-layer (LbL) assembly process using grape seed polyphenol nanoparticles (PNP) and polyelectrolytes (PEs), each applied in two consecutive layers onto a gold-coated sensor crystal.

The preparation of thin multilayer films was monitored by a quartz-crystal microbalance with dissipation (QCM-D) (E4 model, Q sense, Gothenburg, Sweden) to assess the interface compatibility of individual layers. The PE/PNP layer-by-layer assembly was built on a gold sensor as follows: (1) The gold sensor was washed with milli-Q water and the assembled QCM-D cells were washed with milli-Q water for 20 min. (2) The polyelectrolytes were dissolved in 100 mM NaCl and 1 g L^{-1} solutions in the three sets (acidic, neutral and basic pH) were prepared. The assembled QCM-D cells were rinsed with polyelectrolytes for 20 min to coat gold sensors with the first PE layer. (3) The sensors with the first PE layer were washed with milli-Q water for 20 min to remove loosely bound material from the sensors.

https://doi.org/10.1021/acsapm.4c03681
ACS Appl. Polym. Mater. 2025, 7, 3601−3610

(4) The coated sensors were rinsed with PNPs (1 g L^{-1}) for 20 min to secure the second layer. (5) The sensors with two layers were washed with milli-Q water for 20 min to remove loosely bound material from the sensors. (6) The third (PE) and fourth layer (PNPs) were applied to the LbL assembly as in the previous steps. The flow rate applied in all steps was 0.1 mL min^{-1}.

2.2. Characterization Techniques. High-resolution nuclear magnetic resonance (NMR) spectra were recorded in a 5 mm cryoprobe on a Bruker Avance III HD spectrometer at 14 T in deuterated dimethyl sulfoxide (40 °C). Proton and carbon chemical shifts were referenced to tetramethylsilane (TMS). One-dimensional 600 MHz ^{1}H and 150 MHz ^{13}C NMR spectra and two-dimensional Heteronuclear Single Quantum Correlation (HSQC) spectroscopy was used to determine simultaneously the ^{1}H and ^{13}C chemical shifts. HSQC spectra were acquired using a spectral width of 0−12 ppm (^{1}H) and 0−210 ppm (^{13}C), 2048 points in F2, 256 increments (F1; zero-filled to 4K x 1K points) and 128 transients. Spectra were processed by Bruker and MestReNova software. Chemical shifts (δ) are quoted in ppm.

The total phenolic content in PNPs was determined using the Folin−Ciocalteu spectrophotometric method using gallic acid as a reference sample and dimethyl sulfoxide (DMSO) as a solvent.[16]

The weight-average molecular weight (M_w) and dispersity ($Đ$) of the PNPs were determined by Size Exclusion Chromatography (SEC, Infinity 1260, Agilent Technologies) coupled to a Multiangle Laser Light Scattering detection (MALLS, Dawn Heleos II, Wyatt Technology, USA) and a differential refractometer (dRI, Optilab T-rEX, Wyatt Technology). 2 g L^{-1} PNPs were dissolved in DMSO with 0.1% LiBr added to reduce sample aggregation.[30] The sample was filtered through a syringe filter (nylon membrane, pore size 0.45 μm) and analyzed without further treatment.

The particle size distribution, Z-average particle sizes, polydispersity, and ζ-potential of PNPs were determined using a Zetasizer Nano ZS (Malvern Panalytical Ltd., Malvern, U.K.) using dynamic and electrophoretic light scattering. Measurements were conducted at a laboratory temperature (25.0 ± 0.1 °C). All data presented are average values from three independent experiments.

The morphology of PNPs was studied by a JEOL JSM-7600 field-emission scanning electron microscope (FESEM). A dispersion of PNPs at a concentration of approximately 1 g L^{-1} was dropped onto a silicon wafer and allowed to air-dry at room temperature. Images were captured with an accelerating voltage of 5 kV and a magnification of 50,000×.

The viscoelastic properties of thin multilayer films have been investigated using QCM-D. Dissipation changes, ΔD have been used to assess the properties of the adsorbed layers with a focus on the uniformity and compatibility between each layer. The interface compatibility of layers in LbL assemblies can be assessed by the acoustic ratio:

$$\text{acoustic ratio} = \Delta\Gamma/\Delta f \tag{1}$$

where, Γ is the energy dissipation factor ($\Delta\Gamma = \Delta D/2\pi$), D is the dissipation value and f is the value frequency obtained from QCM-D data.

The mass of a thin layer adsorbed on the surface of the neat or coated gold sensor was calculated using the Sauerbrey equation:[31]

$$\Delta m = -\frac{C \times \Delta f}{n} \tag{2}$$

where, m (ng cm^{-2}) is the adsorbed mass per unit area, C (ng cm^{-2} Hz^{-1}) is the mass sensitivity constant ($C \sim 17.7$), Δf (Hz) is the change in frequency and (n) is the overtone number ($n = 3$ for the used equipment).

The morphologies of thin multilayer films were evaluated using AFM. AFM images were collected in tapping mode with a Tosca 400 Atomic Force Microscope (Anton Paar, Graz, Austria) utilizing silicon cantilevers (AP-ARROW-NCR) from Nanoworld AG (Neuchâtel, Switzerland) with a resonance frequency of 285 kHz and a force constant of 42 N m^{-1}. Image processing and calculation of root-mean-square (RMS) roughness were performed with Gwyddion v2.59 software.

The antioxidant activities of PNPs were analyzed using the $ABTS^{\bullet+}$ radical decolorization assay, with 6-hydroxy-2,5,7,8-tetramethylchroman-2-carboxylic acid (Trolox) as a standard.[16] Briefly, 7 mM of ABTS was mixed with 2.45 mM potassium persulfate. The $ABTS^{\bullet+}$ reaction mixture was left in the dark for 12 h at room temperature. The blue-green $ABTS^{\bullet+}$ reaction mixture was then diluted with ethanol to reach an absorbance of 0.70 ± 0.02 at 734 nm. Subsequently, 10 μL of PNP solution was mixed with 990 μL of $ABTS^{\bullet+}$ reaction mixture and left in the dark for 10 min. The absorbance at the beginning of the reaction (A0) and after 10 min (A10) was monitored at 734 nm. The total antioxidant activity was determined by calculating the difference between A0 and A10, which was then plotted against the Trolox calibration curve (25−400 μg mL^{-1}) prepared in 60% ethanol. Free radical scavenging activities of LbL assemblies were examined using a similar methodology but with a gold crystal carrying the LbL assembly immersed in the reaction mixture. Three parallel measurements were performed for each sample to ensure accuracy and reproducibility. The antioxidant activity was expressed as mg Trolox per g of PNP particles and, in the case of films, as μg Trolox per cm^2 of film.

The antibacterial activities of PNPs, poly-L-lysine and thin multilayer films were determined against the Gram-positive bacterium *M. luteus* (CCM 1569) and the Gram-negative bacterium *Escherichia coli* (CCM 8587) supplied by the Czech Collection of Microorganisms (Masaryk University, Brno, Czechia). The antimicrobial activities of materials have been tested as follows:

(1) The broth dilution method was used for the testing of PNPs and poly-L-lysine: samples were incubated at 30 °C for 24 h and the optical density (OD) was analyzed at 600 nm at the beginning of the experiment and after 24 h incubation using the spectrometer-based ELISA reader (BioTek Elx808). At the beginning of each trial, the inoculum was diluted to a final colony concentration of 0.5 McFarland units (approximately 1 × 10^8 cells mL^{-1}). Next, 50 μL of the poly-L-lysine or PNP (0.8 mg mL^{-1}) was added to 150 μL of diluted bacterial suspension in a suitable growth medium to the wells of a sterile 96-well microtiter plate. Diluted inoculum with 50 μL of distilled water was used as a positive control. Each sample was tested in triplicate. The percentage of microbial growth inhibition after 24 h of incubation for the test wells was calculated using the following equation:

$$\text{microbial growth inhibition (\%)} = \frac{\text{OD of control} - \text{OD of test sample}}{\text{OD of control}} \times 100 \tag{3}$$

(2) Similarly, quantitative adsorption method[30] was used to assess the antimicrobial activity of thin multilayer films. Films adhered to the gold sensor were added to the tube with 4 mL of diluted inoculum, with a final colony concentration of 0.5 McFarland units (approximately 1 × 10^8 cells mL^{-1}). The antimicrobial testing was conducted at 30 °C, and the optical density was determined using the spectrometer-based ELISA reader at 600 nm at the beginning of the experiment and after 24 h of incubation. Three parallel measurements of each sample were performed and the percentage of inhibition was calculated using the previous formula 3.

The data of antibacterial activity of PNPs, poly-L-lysine and thin multilayer films were analyzed from the point of view of statistical significance by the analysis of variance employing Origin (version Origin Pro 2019). The Tukey test's differences among mean values were processed at a level of significance of $p < 0.05$.

3. RESULTS AND DISCUSSION

3.1. Properties of Polyphenol Nanoparticles (PNPs). Grape seed lignin is a fine brown powder with particles ranging

https://doi.org/10.1021/acsapm.4c03681
ACS Appl. Polym. Mater. 2025, 7, 3601−3610

from 1 to 10 μm with an irregular shape and a tendency to agglomerate. Therefore, crude GSL lignin is unsuitable for the coating and processing of thin films. However, several authors have demonstrated that lignin nanoparticles and nanospheres can be synthesized from lignin through precipitation from a solution.[32] Figure 3 shows that the transformation of lignin

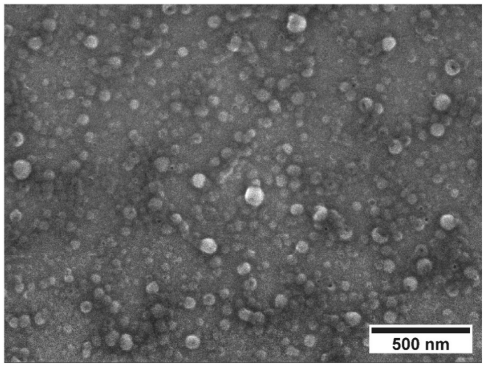

Figure 3. SEM of colloidal polyphenol nanoparticles, obtained at an accelerating voltage of 5 kV and a magnification of 50,000×.

powder into nanoparticles enabled the preparation of spherical-shaped nanoparticles with the intensity-weighted mean hydrodynamic size (Z-average) of 94 ± 4.0 nm and a polydispersity index of 0.18 ± 0.03 (determined by dynamic light scattering).

In line with other authors who found that lignin nanoparticles are readily dispersed in water,[33] the experiments showed that PNP nanoparticles were well dispersed in water. They had an average ζ-potential of −24.1 ± 1.0 mV at pH 7 (Figures S1 and S2). The detected negative value of ζ-potential suggests that the negatively charged PNP nanoparticles should attract positively charged polyelectrolytes and form thin multilayer films with good viscoelastic properties. PNPs reached the M_w of 45.50 ± 6.26 kDa and narrow polydispersity, $Đ$ of 1.13 ± 0.06.

The chemical composition of PNPs was verified by a high-resolution 1D and 2D NMR spectroscopy (Figure 4). Several quite typical resonances for lignin were found in the aromatic region of the 2D HSQC spectra (6−8 ppm for ^{1}H/100−140 ppm for ^{13}C). The main guaiacyl (G) broad signals resonated at 7.05/111.2 ppm (G2), 6.7/114.9 ppm (G5), and 6.8/119 ppm (G6). The syringyl (S2) signal was detected at 7.1/109.7 ppm. The revealed characteristic structural features of lignin correspond with those in the literature.[34] In addition to these typical lignin signals, also other resonances were identified, such as signals at 7.15/125.7 ppm indicating p-hydroxyphenyl unit (H2,6) and weak signals of ferulic acid at 7.45/112.3 ppm (FA2) as well as at 7.2/120.3 ppm (FA6). Next, the verified signal at 7.4/127.7 ppm and 6.85/124.6 ppm showed the presence of p-coumaric acid (PCA) and cinnamaldehyde (Cin), respectively. Trans-cinnamic acid, p-coumaric acid, and ferulic acid are typical for nonwood lignins.[35] The aliphatic part (2.5−6 ppm for ^{1}H/50−90 ppm for ^{13}C) displayed a distinct signal originating from the methoxy (OMe) group (3.75/55.2 ppm). The clear broad group of −O−CH$_2$− signals at 3.50/60.5 ppm originated from the aryl-ether β-O−4 moiety. Additional signals at 3.55/66.5 ppm and 4.75/71.1 ppm correspond with the β-5 −CH$_2$− CA (coniferyl alcohol) group and the interunit α-O−4−CH− group, respectively. The resinol (Res) β−β linkage signal at 3.70/77.1 ppm has been

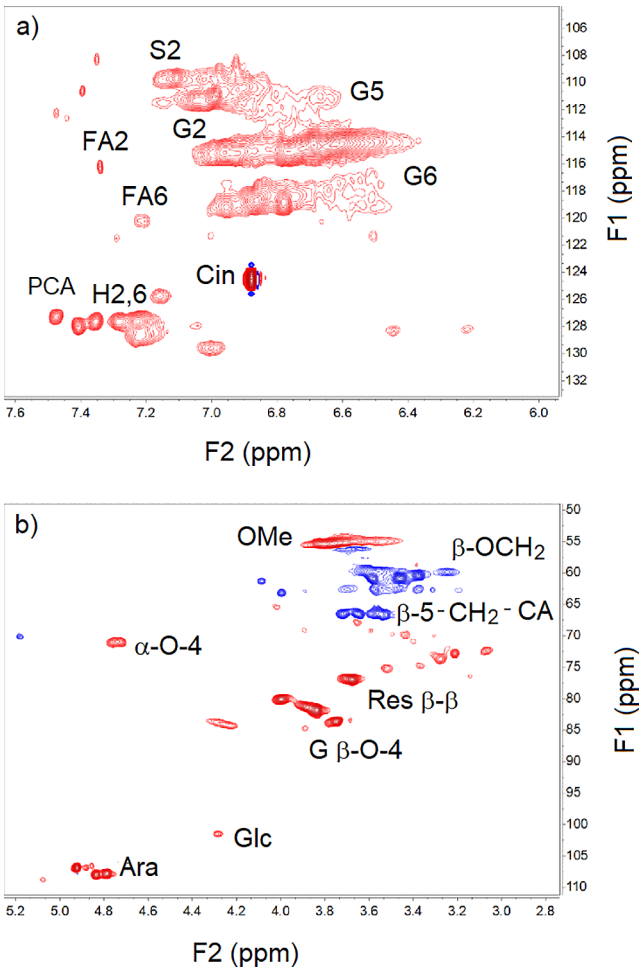

Figure 4. High-resolution 2D NMR HSQC spectra of PNPs isolated from grape seeds collected at 14 T in dimethyl sulfoxide (40 °C) showing (a) aromatic (6−8 ppm for ^{1}H/100−140 ppm for ^{13}C) and (b) aliphatic parts (2.5−6 ppm for ^{1}H/50−115 ppm for ^{13}C). Signals with positive phase (signals originating from methine and methyl groups) are in red, and signals with negative phase (resonances originating from methylene groups) are in blue.

found. The signal at 3.85/81.7 ppm has been assigned to the −CH− signals from the G β−O−4 moiety. Moreover, the signals of carbohydrates α-arabinan at 4.8/107.8 ppm (Ara) and glucan at 4.3/101.7 ppm (Glc) have been identified in the HSQC spectrum. The aromatic and aliphatic parts of the 2D HSQC spectra confirmed the presence of the essential components typical for lignin structures and linkages between lignin, carbohydrates, and other phenolics typical for grape seeds. The determined signals were detected similarly to those reported in other studies.[36−38]

The total phenolic content for PNP particles was 387.6 ± 9.1 mg GAE per gram of PNPs. This amount is about 23.8% higher than that of the original grape seed lignin. Similarly, the quantified ABTS$^{•+}$ radical scavenging activity of PNPs was 433 ± 10 mg Trolox per gram of PNPs, which was about 81.9% higher than that of the original grape seed lignin. The higher content of phenolic substances and the value of the antioxidant capacity of nanoparticles in comparison with the original material were confirmed by other authors.[39] PNPs have demonstrated comparable antioxidant activity to 2,6-di*tert*-butyl-p-cresol (BHT) and lignins recognized for their high radical scavenging power, such as beech wood lignin and

https://doi.org/10.1021/acsapm.4c03681
ACS Appl. Polym. Mater. 2025, 7, 3601−3610

bamboo lignin (Table S2). Specifically, the antioxidant activity of PNPs (433 mg Trolox per gram) is significantly higher than that of acetic acid lignin from bamboo shoot shells (361 mg Trolox per gram), milled wood lignin from bamboo shoot shells (205 mg Trolox per gram), and beech wood lignin (240 mg Trolox per gram) (see Table S2).[40−42] The isolation method applied for lignin is crucial and can significantly enhance its antioxidant activity. For example, in the work of Sun et al.,[41] the steam explosion of bamboo chips followed by alkali delignification resulted in a sample with high antioxidant activity. The alkali fractionated steam exploded bamboo lignin exhibited the highest antioxidant activity among the tested samples, with a value of 727 mg Trolox per gram. Comparing the antioxidant activity of the original grape seed lignin with PNP particles and considering reported values for bamboo lignin modified through different pathways, it can be concluded that both the inherent properties of the lignin source and the applied isolation and modification techniques are key determinants of the resulting antioxidant activity.

PNPs derived from grape seed lignin and poly-L-lysine (PLL) used in this study are known to possess antimicrobial activity.[43,44] PLL is effective against a wide range of microorganisms due to its ability to disrupt the integrity of microbial cell membranes, damage cell walls, and inhibit critical metabolic pathways in bacteria. In contrast, the antibacterial activity of polyphenols, including PNPs, is primarily attributed to their ability to disrupt bacterial walls by accumulating reactive oxygen species on their surface.[45] The antimicrobial activities of PLL and PNPs were determined using the broth dilution test (Figure 5).

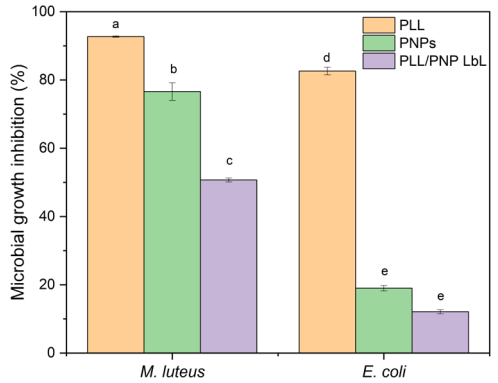

Figure 5. Percentage of microbial growth inhibition obtained for poly-L-lysine (PLL), polyphenol nanoparticles (PNPs), and PLL/PNP LbL against *M. luteus* and *E. coli* after 24 h (average value ± standard deviation, $n = 3$, bars marked by different letters are significantly different, $p < 0.05$).

As hypothesized, poly-L-lysine exhibited high antimicrobial activity against both Gram-positive and Gram-negative bacteria, reducing the bacterial growth of *M. luteus* and *E. coli* by 92.7 ± 0.2% and 82.6 ± 1.1%, respectively. Similarly, PNPs exhibited some antimicrobial activity but primarily against *Gram-positive* bacteria, which possess a less stable bacterial wall structure than *Gram-negative* bacteria. PNPs reduced the bacterial growth of *M. luteus* by 76.6 ± 2.9% and *E. coli* by 19.0 ± 0.8%. The results showing the antimicrobial efficacy of PNPs against *Gram-positive* bacteria and their weak efficacy against *Gram-negative* bacteria are consistent with the findings of other authors (Table S3). Lignins are considered antimicrobial substances; however, their activity varies with chemical structure, molecular weight, chemical reactivity, and solubility.[46]

3.2. Properties of Thin Multilayer Films. The thin multilayer films were prepared by layering on the gold surface using an established LbL technique.[25] The effectiveness of four different, positively charged polyelectrolytes (PAH, PLL, PDM, and PEI, see Figure 1) incorporated as anchor layers to trap negatively charged PNPs has been studied using the QCM-D system. A sequential and controlled deposition of oppositely charged polymers to form thin multilayer films started with the primary layer consisting of polyelectrolyte. The selected polyelectrolytes are characterized by excellent adhesion to gold from which the QCM-D sensor surface is formed.[25] However, PNPs alone do not feature good adhesion to gold surfaces (Figure S3). It is hypothesized that negatively charged polyphenolic PNPs should exhibit strong electrostatic interactions with positively charged polyelectrolytes upon the condition of the favorable pH environment used to prepare LbL systems.[47] Figures S4 and S5 show the values of the adsorbed mass in the individual layers and viscoelastic properties of LbL assemblies. The data obtained from the QCM-D experiments confirmed that the adjustment of pH value for layering is critical due to the strong influence of the environment on the adsorption process. This is true, especially in the case of PAH/PNP and PLL/PNP LbL systems. Exposure of the thin films to the saline polyelectrolyte solutions with different pH values and the extensive rinsing with water after each layer confirm the coating stability. Testing stability upon exposure to harsher conditions (pH value, temperature, salinity) might be necessary for specific applications. The highest mass adsorption of individual polyelectrolytes and PNPs occurs at pH 10, corresponding with the layered materials' chemical structure and pK_a values. At pH10, the basic amine groups in the polyelectrolytes, such as PAH (poly(allylamine hydrochloride)) and PLL (poly-L-lysine), are deprotonated, enhancing their positive charge density.[48] This increased charge density promotes stronger electrostatic interactions with the negatively charged PNPs, primarily composed of lignin and other phenolic compounds. Lignin contains various functional groups, including hydroxyl and carboxyl groups, which can ionize and contribute to the overall negative charge of the PNPs. The deprotonation of these groups at higher pH values further enhances the electrostatic attraction between the PNPs and the polyelectrolytes. PLL, in particular, contains carboxylates from the C-terminal of the peptide, which also contributes to its overall charge and interaction with PNPs (Figure S5 charging isotherms of the PEs). Figure 6 and Table 1 show the frequency and dissipation changes monitored throughout the processing of PAH/PNP, PLL/PNP, PDM/PNP, and PEI/PNP thin multilayer films at pH 10.

A decrease in frequency indicated the mass adsorption of layers based on polyelectrolytes and PNP. The subsequent washing cycle removed the nonabsorbed and loosely bound materials that increased frequency values. The changes in frequencies show that the layering of polyelectrolytes was quick and smooth, unlike the slower gradual adsorption of PNPs owing to their particle nature. Significant repulsion occurred as the surface saturated, leaving limited space for subsequent particle adsorption. Consequently, the adsorption rate decreased due to the necessary rearrangement of molecules on the surfaces with ongoing adsorption. This decrease in

https://doi.org/10.1021/acsapm.4c03681
ACS Appl. Polym. Mater. 2025, 7, 3601−3610

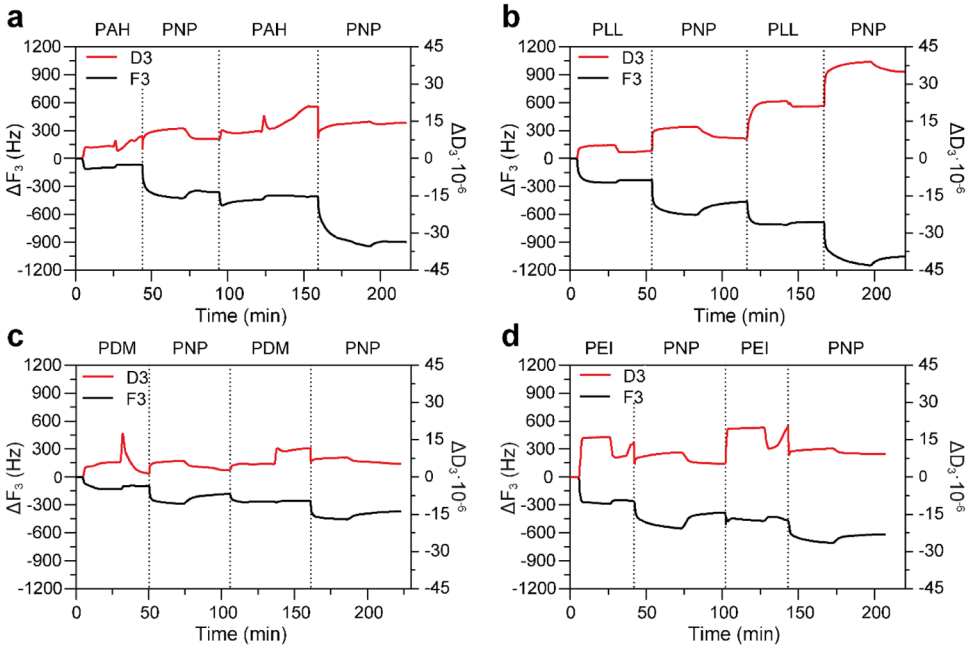

Figure 6. QCM-D measurements for LbL assembly of different polyelectrolytes and PNP at pH 10.0: PAH (a), PLL (b), PDM (c), and PEI (d). The graph shows changes in oscillation frequency (black line, left axis) and energy dissipation (red line, right axis) over time, recorded from the third overtone during the deposition of two bilayers for each system.

Table 1. Mass Adsorption and Viscoelastic Properties of Polyelectrolyte/PNP LbL Assemblies.

sample	ΔD	Δf	m (mg m^{-2})	$\Delta\Gamma$	acoustic ratio
			PAH/PNP LbL		
layer 1	9.150	−63.862	3.77	1.456	−0.023
layer 2	−1.272	−294.732	17.39	−0.202	0.001
layer 3	13.068	−48.586	2.87	2.080	−0.043
layer 4	−6.434	−488.448	28.82	−1.024	0.002
			PLL/PNP LbL		
layer 1	3.055	−230.279	13.59	0.487	−0.002
layer 2	5.017	−231.470	13.66	0.799	−0.003
layer 3	13.025	−221.169	13.05	2.074	−0.009
layer 4	13.677	−364.612	21.51	2.178	−0.006
			PDM/PNP LbL		
layer 1	1.345	−94.475	5.57	0.214	−0.002
layer 2	1.440	−87.400	5.16	0.229	−0.003
layer 3	8.846	−76.284	4.50	1.409	−0.019
layer 4	−6.303	−111.142	6.56	−1.004	0.009
			PEI/PNP LbL		
layer 1	14.143	−257.606	15.20	2.252	−0.009
layer 2	−8.823	−123.147	7.26	−1.405	0.011
layer 3	15.170	−83.629	4.93	2.416	−0.029
layer 4	−11.230	−151.366	8.93	−1.789	0.012

adsorption rate indicates that the surface is becoming saturated with the adsorbed particles, leading to repulsion and rearrangement of the molecules on the surface. Along with the changes in frequency, there were also changes in dissipation during the layering process that exhibited a viscoelastic behavior.[49]

The most consistent dissipation changes exhibited PLL/PNP LbL assembly (Figure 6b). Figure 6a,c,d show different dissipative changes, such as swelling and desorption of the polyelectrolyte during the washing cycle and increasing mass adsorption with the number of steps, especially for PAH and PLL. Therefore, PAH/PNP, PDM/PNP, and PEI/PNP LbL systems show high differences in viscoelastic properties over layers. The variations of ΔD from positive to negative values designate changes in energy dissipation throughout layering due to the formation of softer versus more rigid layers. Similarly, the determined values of the acoustic ratio indicate relatively good interface compatibility between PLL and PNP, especially between the primer PLL layer and the secondary PNP layer (Table 1). The good interface compatibility supported uniform layering of PLL and PNP at similar thicknesses. The rest of the LbL assemblies exhibited significant variations in the values of the acoustic ratios, which was the effect of a less dense packing of the polyelectrolytes caused by the charge density (Figure S5) and nonuniform viscoelastic properties.

Subsequently, the interface properties of LbL assemblies were studied using AFM microscopy. Figure 7 shows the morphologies of the LbL assemblies prepared at pH 10. The PAH/PNP, PLL/PNP, PDM/PNP, and PEI/PNP LbL assemblies exhibited various morphologies. The revealed differences in the surface roughness occurred mainly due to the particle nature of PNPs and their various adhesion ability to the tested polyelectrolytes. The spherical and rigid PNP particles caused the formation of heterostructured multilayer films. The final distribution of particles was influenced mainly by the interface compatibility between them and polyelectrolytes. The morphologies shown in Figure 7 confirmed the poor interfacial interaction between PNP and PAH, PDM, or PEI, as evidenced by the presence of agglomerates. Only the morphology shown in Figure 6b indicates a strong interfacial interaction between PLL and PNP. Due to the strong interfacial interaction, spherical PNP nanoparticles were uniformly distributed on the surface of PLL. The adsorbed mass of PNPs on polyelectrolytes can be assessed by root-mean-square (RMS) roughness values. The highest values of RMS displayed PLL/PNP LbL assembly, indicating about

https://doi.org/10.1021/acsapm.4c03681
ACS Appl. Polym. Mater. 2025, 7, 3601−3610

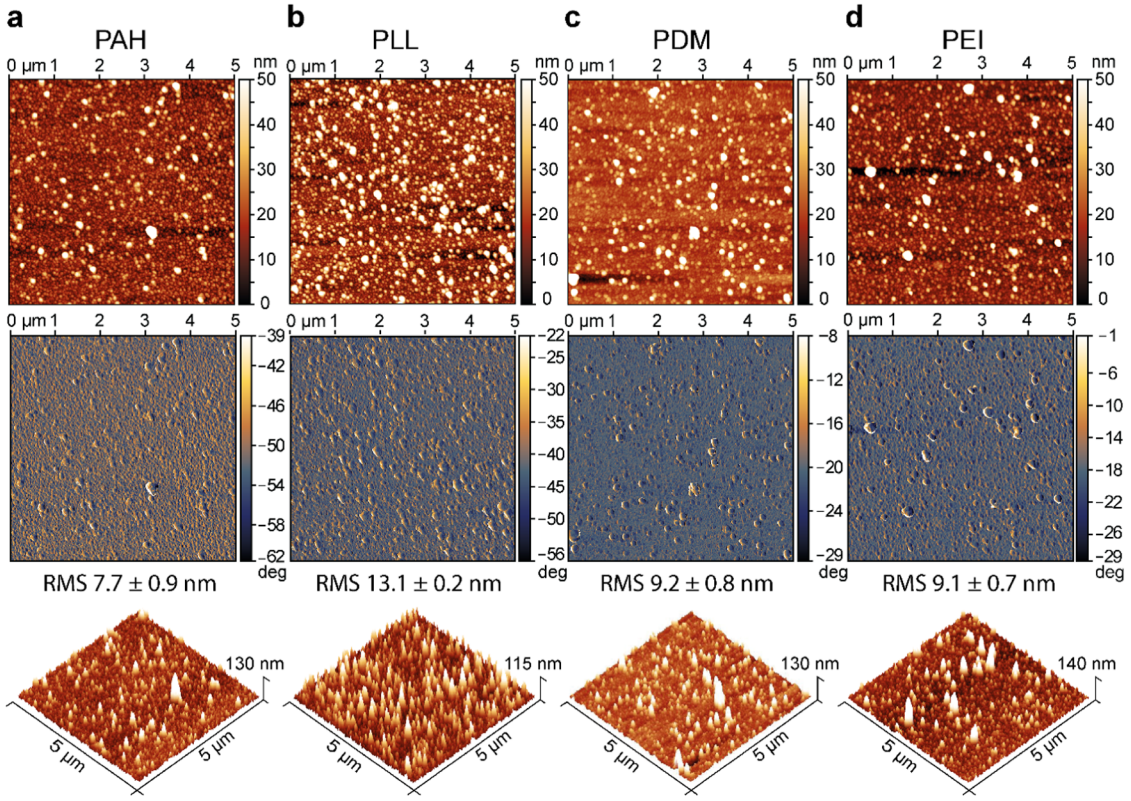

Figure 7. Atomic force microscopy images of LbL assembled polyelectrolytes and PNP at a pH value of 10: PAH (a), PLL (b), PDM (c), and PEI (d). The upper row displays topography.

29.8−41.2% higher content of the adsorbed PNPs compared to the PAH/PNP, PDM/PNP and PEI/PNP assemblies. Higher RMS values show that more PNPs are adsorbed, but it must be noted that the rougher surfaces might give bacteria more places to stick, which could decrease the overall antimicrobial activity of films.[50]

The antioxidant capacities of PNPs in polyelectrolyte/PNP multilayer films were tested using an $ABTS^{\bullet+}$ radical scavenging assay in both acidic and basic environments (Figure 8). The results indicated that the antioxidant activity of the LbL assemblies was higher under alkaline conditions than under acidic conditions, with values ranging from 40 to 71 μg Trolox cm^{-2}. This variation is attributed to the presence of dissociable −OH groups in the polyphenols, which are more active in alkaline environments. Figure 7 shows no significant differences in antioxidant activity among the various films. This indicates that the free radical scavenging activity solely depends on the quantity of hydroxyl groups present on the film surfaces and is independent of the adsorbed mass of PNPs or the character of the previous layer. It can be noted that the influence of the presence of the radical scavenger groups on the layer surface is also evident in the variations observed in films assembled at different pH levels.

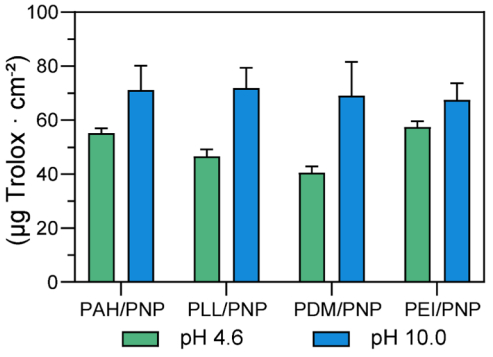

Figure 8. Antioxidant activity of multilayer films composed of polyelectrolytes and grape seed polyphenol nanoparticles (PNP) (bars show average value ± standard deviation, n = 3).

The above-presented data showed that PLL, in combination with PNP, demonstrated the highest adsorbed mass using a layer-by-layer (LbL) assembly methodology. Therefore, this LbL assembly has been selected to test its antimicrobial activity. As we confirmed in the previous section, both materials, PLL and PNPs, display antimicrobial activity, especially against *Gram-positive* bacteria. The antimicrobial activity of PLL/PNP multilayer films with the top layer of PNPs was tested against *M. luteus* and *E. coli* (see Figure 5). After 24 h, the PLL/PNP LbL assembly showed 50.7 ± 0.6% microbial growth inhibition of *M. luteus* and 12.1 ± 0.6% microbial growth inhibition of *E. coli*. The obtained antimicrobial values of the LbL assemblies indicate that the nature of the top layer, which in this case is PNP nanoparticles, determines the resulting antimicrobial activity films.

The investigated polyphenol nanoparticles possess antioxidant and antimicrobial properties; however, they do not adhere well to gold or other surfaces, making it challenging to create stable films. When incorporated into LbL assemblies with polyelectrolytes, especially PLL, PNPs form stable films that can be used as multifunctional coatings on various surfaces. However, forming LbL assemblies requires careful control of pH and other processing conditions to ensure proper layering and stability.

https://doi.org/10.1021/acsapm.4c03681
ACS Appl. Polym. Mater. 2025, 7, 3601−3610

4. CONCLUSIONS

This work showed the synthesis of spherical-shaped polyphenol nanoparticles isolated from grape seeds. The chemical compositions of polyphenol particles studied by NMR spectroscopy confirmed the functional groups typical for lignin and those typical for hydroxycinnamic acids. The presence of ferulic acid, p-coumaric acid, and cinnamaldehyde in PNP particles isolated from grape seed lignin contributed to the final strong antioxidant activity of PNPs. In addition to the radical scavenging activity, the prepared PNPs exhibited antimicrobial activity. These biobased nanoparticles with dual functionality in protecting surfaces from oxidative damage and formation of biofilms could be applicable in various environments, including healthcare, food processing, and consumer products. However, as was presented in this work, PNPs alone do not form stable coatings. Therefore, PNPs were incorporated between different cationic polyelectrolytes. Cationic polyelectrolytes are known to have high adhesion to various types of surfaces, including glass, metal, and plastics. For the formation of stable, thin multilayer films it was essential to achieve good interface compatibility between PNP and the polyelectrolytes. Weak cationic polyelectrolytes with only primary amines (PLL, PAH) showed a higher mass deposition at an increasing pH value, which can be related to denser packing under these conditions. This, in turn, caused the deposition of more PNP on the polyelectrolyte and the formation of stable coatings. The highest masses of PNP were deposited on PLL layers. This enabled the formation of PLL/PNP LbL assemblies with the potential suitability for developing biobased antimicrobial and antioxidative coatings with a low environmental impact.

■ ASSOCIATED CONTENT

Supporting Information

The Supporting Information is available free of charge at https://pubs.acs.org/doi/10.1021/acsapm.4c03681.

Isolation of grape seed lignin; chemical composition of grape seed lignin (GSL); antioxidant activities of BHT and selected lignins; antimicrobial activities of poly-l-lysine and selected lignins; intensity-based radius of polyphenol nanoparticles (PNPs) determined using dynamic light scattering; ζ-potential of PNPs, QCM-D monitoring of PNP layer on a gold surface; QCM-D monitoring of LbL assembly of different polyelectrolytes (PEs) and PNP: PAH pH 4.6 (a), PLL pH 8.0 (b), PDM pH 5.4 (c), and PEI pH 10 (d); the graph shows changes in oscillation frequency (black line, left axis) and energy dissipation (red line, right axis) over time, recorded from the third overtone during the deposition of two bilayers for each system; the titration curves for specific polyelectrolytes PAH (a), PLL (b), PDM (c), and PEI (d) (the upper part); the adsorbed mass of PNP and PE after rinsing calculated according to the Sauerbrey equation are presented for each polyelectrolyte under various pH conditions (the lower part) (PDF)

■ AUTHOR INFORMATION

Corresponding Author

Adriana Kovalcik − *Faculty of Chemistry, Brno University of Technology, 612 00 Brno, Czech Republic;* orcid.org/0000-0003-4833-7369; Email: kovalcik@fch.vut.cz

Authors

Pavel Vostrejs − *Faculty of Chemistry, Brno University of Technology, 612 00 Brno, Czech Republic;* orcid.org/0000-0002-9383-7293

Jana Bianca Schaubeder − *Institute of Bioproducts and Paper Technology, Graz University of Technology, 8010 Graz, Austria*

Stefan Spirk − *Institute of Bioproducts and Paper Technology, Graz University of Technology, 8010 Graz, Austria;* orcid.org/0000-0002-9220-3440

Michal Hricovini − *Institute of Chemistry, Slovak Academy of Sciences, Slovakia, 845 38 Bratislava, Slovakia*

Tiina Nypelö − *Department of Chemistry and Chemical Engineering, Chalmers University of Technology, Gothenburg 41296, Sweden; Department of Bioproducts and Biosystems, Aalto University, Espoo 02150, Finland*

Michal Kalina − *Faculty of Chemistry, Brno University of Technology, 612 00 Brno, Czech Republic;* orcid.org/0000-0002-4224-0841

Nicole Cernekova − *Faculty of Chemistry, Brno University of Technology, 612 00 Brno, Czech Republic*

Matej Brezina − *Faculty of Chemistry, Brno University of Technology, 612 00 Brno, Czech Republic*

Rupert Kargl − *Institute of Chemistry, Graz University of Technology, 8010 Graz, Austria;* orcid.org/0000-0003-4327-7053

Complete contact information is available at: https://pubs.acs.org/10.1021/acsapm.4c03681

Author Contributions

P.V.: investigation, visualization, and writing—original draft. A.K.: conceptualization, supervision, validation, and writing—original draft, review, and editing. J.B.S.: investigation, methodology, and validation. S.S.: conceptualization, validation, and writing—editing. M.H.: investigation, methodology, and validation. T.N.: investigation, methodology, and writing—editing. M.K.: investigation, and methodology. N.C.: investigation, and methodology. M.B.: investigation, and methodology. R.K.: conceptualization, validation, and writing—editing.

Notes

The authors declare no competing financial interest.

■ ACKNOWLEDGMENTS

P.V. and A.K. acknowledge funding through the internal scientific grant of Brno University of Technology (FCH-S-24-8526). Moreover, the authors thank Mika Sipponen from Stockholm University for help with fractionation of the grape seed polyphenols.

■ REFERENCES

(1) Caselli, E.; D'Accolti, M.; Soffritti, I.; Lanzoni, L.; Bisi, M.; Volta, A.; Berloco, F.; Mazzacane, S. An Innovative Strategy for the Effective Reduction of MDR Pathogens from the Nosocomial Environment. In *Advances in Microbiology, Infectious Diseases and Public Health*; Donelli, G., Ed.; Springer International Publishing, 2019; Vol. *13*, pp 79−91.

(2) Page, K.; Wilson, M.; Parkin, I. P. Antimicrobial surfaces and their potential in reducing the role of the inanimate environment in the incidence of hospital-acquired infections. *J. Mater. Chem.* **2009**, *19* (23), 3819−3831.

(3) Dhanasekaran, D.; Thajuddin, N.; Panneerselvam, A. *Antimicrobials: Synthetic and Natural Compounds*; CRC Press, 2015.

(4) Rodrigues, A. E.; de Oliveira Rodrigues Pinto, P. C.; Barreiro, M. F.; da Costa, C. A. E.; da Mota, M. I. F.; Fernandes, I. *An Integrated Approach for Added-Value Products from Lignocellulosic Biorefineries: Vanillin, Syringaldehyde, Polyphenols and Polyurethane*; Springer International Publishing, 2018.
(5) Sholahuddin, S.; Arinawati, D. Y.; Nathan, V. K.; Asada, C.; Nakamura, Y. Antioxidant and antimicrobial activities of lignin-derived products from all steam-exploded palm oil mill lignocellulosic biomass waste. *Chem. Biol. Technol. Agric.* **2024**, *11*, No. 5.
(6) Lattanzio, V. Phenolic Compounds: Introduction. In *Natural Products: Phytochemistry, Botany and Metabolism of Alkaloids, Phenolics and Terpenes*; Ramawat, K. G.; Mérillon, J. M., Eds.; Springer: Berlin Heidelberg, 2013; pp 1543−1580.
(7) Duba, K. S.; Casazza, A. A.; Mohamed, H. B.; Perego, P.; Fiori, L. Extraction of polyphenols from grape skins and defatted grape seeds using subcritical water: Experiments and modeling. *Food Bioprod. Process.* **2015**, *94*, 29−38.
(8) Yedro, F. M.; García-Serna, J.; Cantero, D. A.; Sobrón, F.; Cocero, M. J. Hydrothermal hydrolysis of grape seeds to produce bio-oil. *RSC Adv.* **2014**, *4* (57), 30332−30339.
(9) Yedro, F. M.; García-Serna, J.; Cantero, D. A.; Sobrón, F.; Cocero, M. J. Hydrothermal fractionation of grape seeds in subcritical water to produce oil extract, sugars and lignin. *Catal. Today* **2015**, *257*, 160−168.
(10) Bagchi, D.; Bagchi, M.; Stohs, S. J.; Ray, S. D.; Sen, C. K.; Preuss, H. G. Cellular protection with proanthocyanidins derived from grape seeds. *Ann. N. Y. Acad. Sci.* **2002**, *957* (1), 260−270.
(11) Kim, S.-Y.; Jeong, S.-M.; Park, W.-P.; Nam, K. C.; Ahn, D. U.; Lee, S.-C. Effect of heating conditions of grape seeds on the antioxidant activity of grape seed extracts. *Food Chem.* **2006**, *97* (3), 472−479.
(12) Spigno, G.; Marinoni, L.; Garrido, G. D. 1 - State of the Art in Grape Processing By-Products. In *Handbook of Grape Processing By-Products*; Galanakis, C. M., Ed.; Academic Press, 2017; pp 1−27.
(13) Yilmaz, Y.; Toledo, R. T. Health aspects of functional grape seed constituents. *Trends Food Sci. Technol.* **2004**, *15* (9), 422−433.
(14) Kovalcik, A.; Pernicova, I.; Obruca, S.; Szotkowski, M.; Enev, V.; Kalina, M.; Marova, I. Grape winery waste as a promising feedstock for the production of polyhydroxyalkanoates and other value-added products. *Food Bioprod. Process.* **2020**, *124*, 1−10.
(15) Prozil, S. n. O.; Evtuguin, D. V.; Silva, A. M.; Lopes, L. P. Structural characterization of lignin from grape stalks (*Vitis vinifera* L.). *J. Agric. Food Chem.* **2014**, *62* (24), 5420−5428.
(16) Vostrejs, P.; Adamcova, D.; Vaverkova, M. D.; Enev, V.; Kalina, M.; Machovsky, M.; Sourkova, M.; Marova, I.; Kovalcik, A. Active biodegradable packaging films modified with grape seeds lignin. *RSC Adv.* **2020**, *10* (49), 29202−29213.
(17) Koshijima, T.; Watanabe, T. *Association Between Lignin and Carbohydrates in Wood and Other Plant Tissues*; Springer, 2003.
(18) Sameni, J.; Krigstin, S.; Sain, M. Solubility of lignin and acetylated lignin in organic solvents. *BioResources* **2016**, *12* (1), 1548−1565.
(19) Steck, J.; Junker, F.; Eichhöfer, H.; Bunzel, M. Chemically different but often mistaken phenolic polymers of food plants: Proanthocyanidins and lignin in seeds. *J. Agric. Food Chem.* **2022**, *70* (37), 11704−11714.
(20) Österberg, M.; Sipponen, M. H.; Mattos, B. D.; Rojas, O. J. Spherical lignin particles: a review on their sustainability and applications. *Green Chem.* **2020**, *22* (9), 2712−2733.
(21) Borrega, M.; Päärnilä, S.; Greca, L. G.; Jääskeläinen, A.-S.; Ohra-Aho, T.; Rojas, O. J.; Tamminen, T. Morphological and wettability properties of thin coating films produced from technical lignins. *Langmuir* **2020**, *36* (33), 9675−9684.
(22) Hoeger, I. C.; Filpponen, I.; Martin-Sampedro, R.; Johansson, L.-S.; Osterberg, M.; Laine, J.; Kelley, S.; Rojas, O. J. Bicomponent lignocellulose thin films to study the role of surface lignin in cellulolytic reactions. *Biomacromolecules* **2012**, *13* (10), 3228−3240.
(23) Moradipour, M.; Tong, X.; Novak, B.; Kamali, P.; Asare, S. O.; Lynn, B. C.; Moldovan, D.; Rankin, S. E.; Knutson, B. L. Interaction of lignin dimers with model cell membranes: A quartz crystal microbalance and molecular dynamics simulation study. *Biointerphases* **2021**, *16* (4), No. 041003, DOI: 10.1116/6.0001029.
(24) Alipoormazandarani, N.; Benselfelt, T.; Wang, L.; Wang, X.; Xu, C.; Wågberg, L.; Willfor, S.; Fatehi, P. Functional lignin nanoparticles with tunable size and surface properties: fabrication, characterization, and use in layer-by-layer assembly. *ACS Appl. Mater. Interfaces* **2021**, *13* (22), 26308−26317.
(25) Norgren, M.; Gärdlund, L.; Notley, S. M.; Htun, M.; Wågberg, L. Smooth model surfaces from lignin derivatives. II. Adsorption of polyelectrolytes and PECs monitored by QCM-D. *Langmuir* **2007**, *23* (7), 3737−3743.
(26) Ushimaru, K.; Morita, T.; Fukuoka, T. A bio-based adhesive composed of polyelectrolyte complexes of lignosulfonate and cationic polyelectrolytes. *J. Wood Chem. Technol.* **2020**, *40* (3), 172−177.
(27) Gu, L.; Xie, M.-Y.; Jin, Y.; He, M.; Xing, X.-Y.; Yu, Y.; Wu, Q.-Y. Construction of antifouling membrane surfaces through layer-by-layer self-assembly of lignosulfonate and polyethyleneimine. *Polymers* **2019**, *11* (11), No. 1782.
(28) Sipponen, M. H.; Smyth, M.; Leskinen, T.; Johansson, L.-S.; Österberg, M. All-lignin approach to prepare cationic colloidal lignin particles: stabilization of durable Pickering emulsions. *Green Chem.* **2017**, *19* (24), 5831−5840.
(29) Ristić, T.; Mohan, T.; Kargl, R.; Hribernik, S.; Doliška, A.; Stana-Kleinschek, K.; Fras, L. A study on the interaction of cationized chitosan with cellulose surfaces. *Cellulose* **2014**, *21*, 2315−2325.
(30) Saunders, G.; MacCreath, B. *Artifact Free Analysis of Lignins by GPC using Agilent PolarGel-M.*; Agilent Technologies, Inc, 2024. (accessed July 3, 2024).
(31) Sauerbrey, G. Verwendung von Schwingquarzen zur Wägung dünner Schichten und zur Mikrowägung. *Top. Catal.* **1959**, *155* (2), 206−222.
(32) Ruwoldt, J.; Blindheim, F. H.; Chinga-Carrasco, G. Functional surfaces, films, and coatings with lignin−a critical review. *RSC Adv.* **2023**, *13* (18), 12529−12553.
(33) Pinho, E.; Magalhães, L.; Henriques, M.; Oliveira, R. Antimicrobial activity assessment of textiles: standard methods comparison. *Ann. Microbiol.* **2011**, *61*, 493−498.
(34) Yelle, D. J.; Broda, M. Characterizing the chemistry of artificially degraded Scots pine wood serving as a model of naturally degraded waterlogged wood using1H−13C HSQC NMR. *Wood Sci. Technol.* **2025**, *59* (1), No. 8.
(35) Ralph, J.; Lundquist, K.; Brunow, G.; Lu, F.; Kim, H.; Schatz, P. F.; Marita, J. M.; Hatfield, R. D.; Ralph, S. A.; Christensen, J. H.; Boerjan, W. Lignins: natural polymers from oxidative coupling of 4-hydroxyphenyl-propanoids. *Phytochem. Rev.* **2004**, *3*, 29−60.
(36) Balakshin, M.; Capanema, E.; Gracz, H.; Chang, H.-m.; Jameel, H. Quantification of lignin−carbohydrate linkages with high-resolution NMR spectroscopy. *Planta* **2011**, *233*, 1097−1110.
(37) Wen, J.-L.; Xue, B.-L.; Xu, F.; Sun, R.-C. Unveiling the structural heterogeneity of bamboo lignin by in situ HSQC NMR technique. *Bioenerg. Res.* **2012**, *5*, 886−903.
(38) Kousika, R.; Pu, Y.; Hoey, M.; Holwerda, E.; Bomble, Y.; Hengge, N.; Ragauskas, A. *Heteronuclear Single Quantum Coherence (HSQC) NMR Spectra of Lignin Isolated from Switchgrass Residues after Fermentation with Milling*; Oak Ridge National Laboratory (ORNL): Oak Ridge, TN (United States), 2024.
(39) Trevisan, H.; Rezende, C. A. Pure, stable and highly antioxidant lignin nanoparticles from elephant grass. *Ind. Crops Prod.* **2020**, *145*, No. 112105.
(40) Gong, W.; Xiang, Z.; Ye, F.; Zhao, G. Composition and structure of an antioxidant acetic acid lignin isolated from shoot shell of bamboo (*Dendrocalamus latiforus*). *Ind. Crops Prod.* **2016**, *91*, 340−349.
(41) Sun, S.-N.; Cao, X.-F.; Xu, F.; Sun, R.-C.; Jones, G. L. Structural features and antioxidant activities of lignins from steam-exploded bamboo (*Phyllostachys pubescens*). *J. Agric. Food Chem.* **2014**, *62* (25), 5939−5947.

(42) Rumpf, J.; Burger, R.; Schulze, M. Statistical evaluation of DPPH, ABTS, FRAP, and Folin-Ciocalteu assays to assess the antioxidant capacity of lignins. *Int. J. Biol. Macromol.* **2023**, *233*, No. 123470.
(43) Daglia, M. Polyphenols as antimicrobial agents. *Curr. Opin. Biotechnol.* **2012**, *23* (2), 174−181.
(44) Hyldgaard, M.; Mygind, T.; Vad, B. S.; Stenvang, M.; Otzen, D. E.; Meyer, R. L. The antimicrobial mechanism of action of epsilon-poly-l-lysine. *Appl. Environ. Microbiol.* **2014**, *80* (24), 7758−7770.
(45) Li, K.; Zhong, W.; Li, P.; Ren, J.; Jiang, K.; Wu, W. Antibacterial mechanism of lignin and lignin-based antimicrobial materials in different fields. *Int. J. Biol. Macromol.* **2023**, *252*, No. 126281.
(46) Dong, X.; Dong, M.; Lu, Y.; Turley, A.; Jin, T.; Wu, C. Antimicrobial and antioxidant activities of lignin from residue of corn stover to ethanol production. *Ind. Crops Prod.* **2011**, *34* (3), 1629−1634.
(47) Yin, Z.; Zheng, T.; Ho, C.-T.; Huang, Q.; Wu, Q.; Zhang, M. Improving the stability and bioavailability of tea polyphenols by encapsulations: a review. *Food Sci. Hum. Wellness* **2022**, *11* (3), 537−556.
(48) Stobiecka, M.; Hepel, M. Double-shell gold nanoparticle-based DNA-carriers with poly-L-lysine binding surface. *Biomaterials* **2011**, *32* (12), 3312−3321.
(49) Kolman, K.; Makowski, M. M.; Golriz, A. A.; Kappl, M.; Pigłowski, J.; Butt, H.-J.r.; Kiersnowski, A. Adsorption, aggregation, and desorption of proteins on smectite particles. *Langmuir* **2014**, *30* (39), 11650−11659.
(50) Chen, G.; Wang, Z.; Wang, H.; Zhao, X.; Hu, J.; Wang, S.; Zhang, S. Effects of tetrahedral amorphous carbon film deposited on dental cobalt−chromium alloys on bacterial adhesion. *Surf. Coat. Technol.* **2012**, *206* (15), 3386−3392.

https://doi.org/10.1021/acsapm.4c03681
ACS Appl. Polym. Mater. 2025, 7, 3601−3610